

Pressure-induced phase transition of isoreticular MOFs: Mechanical instability due to ligand buckling

Penghua Ying, Jin Zhang ^{**}, Zheng Zhong ^{*}

School of Science, Harbin Institute of Technology, Shenzhen, 518055, PR China



ARTICLE INFO

Keywords:

Isoreticular Metal-organic-framework
Pressure-induced transitions
DUT materials
IRMOF materials
Mechanical stability
Ligand buckling

ABSTRACT

Since MOFs are often upon varied pressures in gas adsorption/desorption process, understanding the mechanical stability of these ultraporous frameworks becomes extremely crucial. In this paper, taking the isoreticular DUT material as an example, the relation between the mechanical stability of isoreticular MOFs and their ligands is investigated by real-time molecular dynamics simulations as well as three state of art computational approaches including Born stability criteria, anisotropy in elastic moduli and pressure-versus-volume equations. It is found that the global instability of DUT materials is driven by the local buckling of their ligand backbones. Inspired by this finding, we develop here a mechanical model based on three parameters including the topology constant, the elastic modulus of ligand and the ligand length. Through comparing to the results extracted from computational methods, it is found that our mechanical model is reliable in describing the critical transition pressure of various isoreticular MOF materials such as DUT and IRMOF materials. The mechanical model developed here not only provides a design criterion for isoreticular MOF crystals to modify their rigid/flexible properties, but also can be utilized to give a quick prediction of the critical transition pressure of isoreticular MOFs.

1. Introduction

In 2002, Yaghi's group designed a series of isoreticular metal-organic-framework (MOF) crystals [1], i.e., IRMOF family. In their pioneering work, IRMOF-1 (i.e., MOF-5) was taken as a prototype to functionalize the organic groups or extend the organic ligands. Since then, this approach of reticular synthesis [2] has been widely adopted for the assembly of ordered frameworks to achieve precise functional applications. In the synthesis of MOFs, the modifications in the organic ligand linker can adjust the flexible/rigid nature of isoreticular MOF crystals. For example, Chaplais et al. [3] reported that ZIF-8 can transform from flexible to rigid property when its conventional imidazolate linker substitution CH_3 is replaced by Br. The flexibility of ZIF-8, however, can be retained if the imidazolate linker substitution is Cl. Under this circumstance, the functional group substitution in ZIF-8 materials has a profound impact on their energetic performances [4], adsorptive properties [3] and thermal transports [5], since these properties depend on the flexible/rigid nature of ZIF-8. By increasing the ligand length, Krause et al. [6] proposed a general network architecture design criterion for the negative gas adsorption (NGA) transition in DUT materials.

The flexible property or the mechanical stability of the constructed DUT series upon pressure is found to be dependent on their ligand backbone. In addition, among these new isoreticular DUT materials, DUT-50 is found to possess NGA, which is similar to its DUT-49 counterpart observed before [7]. The similar method is also employed to generate other isoreticular series of MOFs such as MIL-140 series [8,9], UiO series and NU-900 series [10].

As stated above, the organic ligand linker in MOF crystals plays a very important role in determining their mechanical response when MOF crystals are subjected to physical stresses [11]. Most existing studies [10,12–16] mainly focused on the elastic modulus of MOF crystals, since it determines the robust practical applications of MOFs. In addition to the elastic modulus, the stability is also important for the reliable scale-up production of flexible MOF crystals in industrial applications, because the densification procedure upon pressure is required in the large-scale fabrication of MOF materials [17]. Compared to the conventional porous materials such as zeolites, flexible MOF crystals usually possess a relatively low stability, since the critical transition pressure of flexible MOF crystals under compression is in the order of 10 MPa [18]. However, in the industrial practice, the pressure

* Corresponding author.

** Corresponding author.

E-mail addresses: jinzhang@hit.edu.cn (J. Zhang), zhongzheng@hit.edu.cn (Z. Zhong).

with a magnitude of 100 MPa is usually employed in the densification procedure of MOFs [17]. To date, considerable efforts have been made to evaluate the elastic moduli of MOFs; however, the study on the mechanical stability of MOF crystals is still in its infancy stage. In spite of several experimental reports [19–24], the computational approaches are widely employed in investigating the mechanical stability of MOF crystals under compression [12,18,22,23,25–30]. These computational approaches include *ab initio* calculations and classical molecular dynamics (MD) simulations [31]. Compared with computationally expensive *ab initio* calculations, classical MD simulations have advantages of modelling MOFs at a larger spatial and longer time scale, which thus are widely used in existing studies. To date, MD simulations have been incorporated in many computational methods to determine the mechanical stability of MOFs from different aspects, which include the Born stability criteria [32], the anisotropy in elastic moduli [33], and the pressure-versus-volume equations of state (P - V EOS) [34–36]. Recently, Rogge et al. [37] presented a comprehensive review on the comparison among these existing computational methods determining the mechanical stability of MOFs. Their study suggests that the MOFs whose pressure-induced transition (PIT) occurs at the pressure below 100 MPa are defined as flexible MOFs, while others are defined as rigid MOFs [37]. Although numerous computational approaches have been developed, there is no general rule describing the relationship between the mechanical instability of MOFs and their structures. Hence, a theoretical model that can evaluate the mechanical stability of MOFs is indispensable for their practical applications.

To this end, the PIT of five isoreticular DUT crystals (DUT-48, -46, -49, -50, and -151) is comprehensively investigated in this work. The organization of this work is briefly shown in Fig. 1. We first employ four

computational approaches including real-time MD simulations, Born stability criteria, the anisotropy in elastic moduli, and P - V EOS to investigate the PIT of isoreticular DUT materials (see Fig. 1(a–d)). Based on the results obtained from molecular simulations, we find that the global instability of DUT materials is driven by the local buckling of their ligand backbones, which indicates that the critical transition pressure is strongly dependent on the ligands. We further find that the relation between the critical transition pressure and the ligands obeys the well-known Euler law, which is often utilized in analyzing the instability of a slender column under compression (see Fig. 1(e)). This finding is also verified by another isoreticular MOF, i.e., IRMOFs. Based on structural mechanics together with the computational results, we finally develop an analytic model to unravel the nature behind the mechanical instability of isoreticular DUTs (see Fig. 1(f)).

2. Computational methods

2.1. Crystal models

Five isoreticular DUT materials including DUT-49 (Fig. 2(a)) and four DUT-49 derivatives, i.e., DUT-46, -49, -50 and -151 in Fig. 2(b) are investigated here. The atomistic models constructed for MD simulations were extracted from the original synthetic report [6]. As shown in Fig. 2(b), the length of ligand backbone of all considered isoreticular DUT materials increases following the order of DUT-48, -46, -49, -50 and -151. It is noted that the ligand backbone of DUT-48 (L_1), -49 (L_3), -50 (L_4) and -151 (L_5) is, respectively, composed of one, two, three and four units of 1,4-substituted phenylene, while DUT-46 (L_2) has a 2, 6-substituted naphthalene making it possess an intermediate length

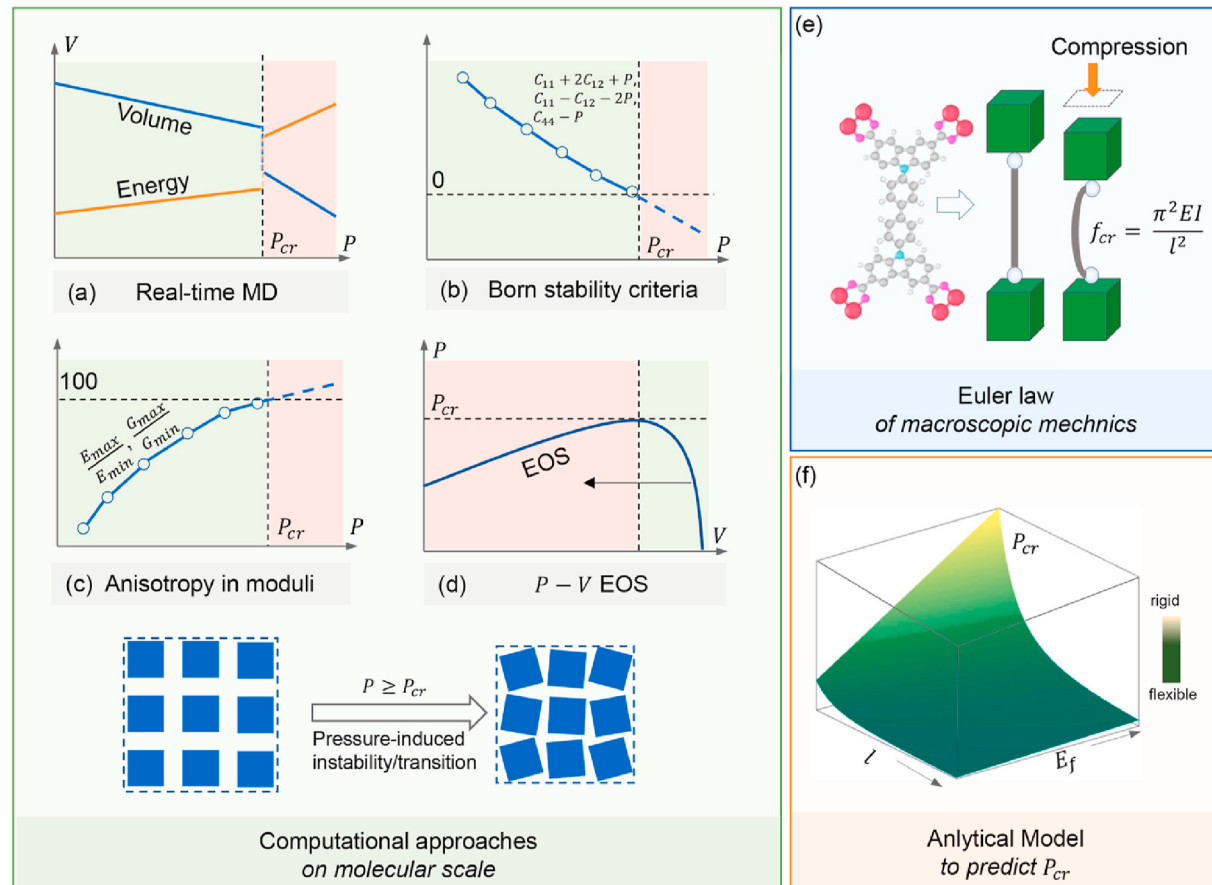


Fig. 1. (a) Real-time MD simulations, (b) Born stability criteria, (c) anisotropy in elastic moduli, and (d) P - V EOS employed here to evaluate the critical transition pressure P_{cr} of MOFs. (e) The Euler law from macroscopic mechanics, which is adopted to investigate the buckling behavior of ligands. (f) A mechanical model developed here to predict P_{cr} of MOF crystals, which is based on the computational approaches and Euler law.

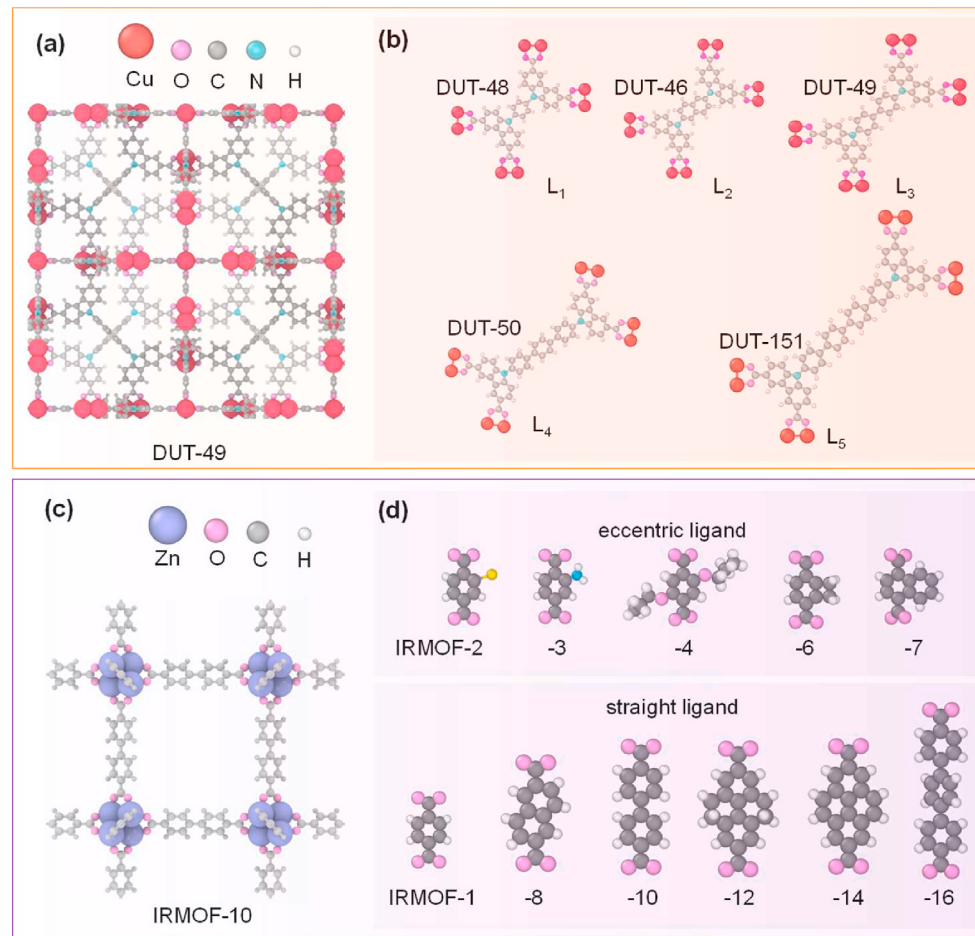


Fig. 2. (a) Atomistic structures of $2 \times 2 \times 2$ supercells of DUT-49. Cu, O, C, N and H atoms are colored in red, purple, gray, azure and white, respectively. (b) Ligands of DUT-48, -46, -49, -50 and 151. (c) Atomistic structures of $2 \times 2 \times 2$ supercells of IRMOF-10. Zn, O, C, N and H atoms are colored in blue, purple, gray and white, respectively. (d) Ligands of IRMOF-2 through -16. Here, all ligands are divided into two groups: the eccentric ligands of IRMOF-2 through -7, and the straight ligand of other IRMOFs. (For interpretation of the references to color in this figure legend, the reader is referred to the Web version of this article.)

between DUT-48 and DUT-49. The interactions between atoms in DUT materials are described by the first-principles derived MOF-FF force field [6,38]. This force-field has been successfully utilized to reproduce the unit-cell parameters of DUT-49 and its derivatives measured in experiments [39]. Through MD simulations together with this force field, the NGA phenomena also have been repeated [6,39].

The initial structural parameters such as lattice length, ligand length, porosity, and the largest pore diameter of isoreticular DUT materials are listed in Table 1. Here, the lattice length was calculated at room temperature (300 K), which is slightly smaller than the value reported at 0 K in Ref. [6]. This difference can be attributed to the negative thermal expansion usually existing in isoreticular DUT materials [40]. The ligand length is defined as the N–N distance of the ligand backbone in Fig. 2(b). The porosity and the largest pore diameter were calculated by the Zeo++ code [41,42] with the probe sphere radius being set as 2.0 Å. The

structural parameters listed in Table 1 clearly illustrate the impact of ligand substitution on the general network design of ultraporous frameworks. In general, when the length of ligand backbone increases from DUT-48 to -151, a nearly linear growth is found in the lattice length, porosity, and the largest pore diameter.

Eleven isoreticular IRMOFs (IRMOF-1, -2, -3, -4, -6, -7, -8, -10, -12, -14, and -16) are also considered in this study, which are treated as supplements of aforementioned DUT materials to further reveal the general relation between the mechanical instability of isoreticular MOFs and their ligand backbone. The crystal structures of IRMOF series considered here were extracted from Ref. [1]. Another four double interpenetrating structures (IRMOF-9, -11, -13, and -15) and IRMOF-5 reported in Ref. [1] are excluded in our work. The crystal structures and ligand configurations of eleven investigated IRMOF materials are shown in Fig. 2(c) and (d), respectively, while their crystal parameters are listed in Table S1. Considering the fact that abundant organic linkers exist in these IRMOFs, the UFF4MOF force field [43] is employed in the present MD simulations. In addition to the easily transferable feature, this forcefield also provides an accurate prediction of the bulk modulus and thermal expansion coefficient of IRMOF series such as IRMOF-1 and IRMOF-10 [43]. Hence, this forcefield is believed to be reliable in qualitatively examining the ligand-dependent stability of IRMOF materials upon pressure. The LAMMPS-interface code tool [43] is used here to prepare the input files for MD simulations of IRMOF materials.

Table 1
Structure parameters of isoreticular DUT materials.

DUT series	Atom numbers	Lattice length (Å)	Ligand length (Å)	Porosity	Largest pore diameter (Å)
DUT-48	1488	40.5	5.6	0.79	18.3
DUT-46	1632	43.9	7.9	0.81	21.4
DUT-49	1728	46.7	10.0	0.84	24.3
DUT-150	1968	52.6	14.3	0.87	30.1
DUT-151	2208	58.7	18.7	0.90	36.2

2.2. Computational methods

All MD simulations were performed by using the publicly available simulation code LAMMPS [44]. Here, the standard Newton equations of

motion were integrated in time by using the velocity Verlet algorithm with a time step of 1.0 fs. Unless otherwise specified, all MD simulations were performed at the room temperature of 300 K. Four kinds of computational methods were adopted in the present study to evaluate the mechanical stability of MOFs under the hydrostatic pressure, which include real-time MD simulations, Born stability criteria, anisotropy in elastic moduli, and *P*-*V* EOS. The schematic overview of these computational methods is graphically shown in Fig. 1(a)–(d). Specifically, the instability or phase transition of crystals can be directly observed in real-time MD simulations by gradually increasing the pressure at a fixed rate in simulations.

Due to high symmetry, the Born stability criteria for cubic crystals under the hydrostatic pressure *P* can be simplified as [45].

$$C_{11} + 2C_{12} + P \geq 0$$

$$C_{11} - C_{12} - 2P \geq 0$$

$$C_{44} - P \geq 0 \quad (1)$$

where C_{11} , C_{12} , and C_{44} are moduli for axial compression, dilation on compression, and shearing, respectively.

The criterion of anisotropy in elastic moduli can be written as [33].

$$A = \max \left\{ G_{\max}/G_{\min}, E_{\max}/E_{\min} \right\} < 100 \quad (2)$$

Here, A is the anisotropic ratio of elastic modulus, which represents the degree of anisotropic. G_{\max} and G_{\min} represent the maximum and minimum values of shear modulus, respectively. Similarly, E_{\max} and E_{\min} are the maximum and minimum Young's modulus along axial direction, respectively.

For *P*-*V* EOS method, the transition of the slope of pressure (*P*)-volume (*V*) from negative to positive as shown in Fig. 1(d) denotes the thermodynamically transition from stable state to unstable state. Hence, the instability criteria could be written as [34].

$$\frac{\partial P}{\partial V} \geq 0 \quad (3)$$

In the above discussion we just present a brief introduction to the criteria of four computational methods employed here. The theories and more computational details of these four computational methods are provided in the supplementary materials. In addition, we also refer the readers to the paper by Rogge et al. [37] for additional examples and detailed discussion.

First-principles calculations were conducted here to calculate the Young's modulus of ligands in IRMOFs series. All first-principles calculations were based on the density functional theory, which were implemented by the CASTEP package [46] together with the generalized gradient approximation of the Perdew-Burke-Ernzerhof functional form [47]. A 400 eV cutoff was employed for the plane wave basis. In the present calculations, the convergence threshold was set as 10^{-6} eV in energy and 10^{-3} eV/Å in force.

3. Results and discussion

3.1. PIT of DUT materials by computational approaches

Isoreticular DUTs exhibit the attractive NGA phenomenon, which is closely related to their designable flexible property. In previous studies, the flexibility feature of MOF crystals is found to be characterized by some of their mechanical properties such as bulk modulus [10], anisotropy in elastic properties [33], and the transition of thermodynamic equation [34]. In what follows, four computational approaches introduced above are adopted to investigate the PIT of DUT materials. Special efforts are made to clarify the relation between the flexible property of DUT materials and their aforementioned mechanical

properties. Meanwhile, the dependence of mechanical behaviors of DUT materials on the extended organic linker and the pressure is carefully examined.

(i) Real-time MD simulations

We first perform real-time MD simulations on the isoreticular DUT materials to investigate their mechanical stability under compression. In doing this, volume, pressure, and internal energy of these MOF materials are calculated, which are extracted by averaging values in MD simulations every 100 ps to avoid the effect of thermal fluctuation. The structure evolution of DUT-48, DUT-49 and DUT-151 during the loading process is plotted in Fig. 3, while the result of other two DUT materials (DUT-46 and DUT-50) is plotted in Fig S1. As shown in Fig. 3(a) and Fig S1(a), a shrinkage in the volume is found in all five DUT materials when the applied pressure is in the range from 0 to 50 MPa. The corresponding internal energy evolution of these five DUT materials during the loading process is plotted in Fig S2, which is found to be in accordance with the volume change shown in Fig. 3(a). The abrupt drop of volume in Fig. 3(a) (or the corresponding abrupt increase of energy in Fig S2) represents the occurrence of phase transition. Three distinct phases including the open pore (*op*) phase, the closed pore (*cp*) phase and the dense phase are successively found in DUT materials during the loading process. Upon the unloading process, i.e., the release of pressure, DUT materials retain the *cp* phases rather than fully recover to the initial *op* phases (see Movie S1-S5 in supplementary materials). As for all five DUT materials, the internal energy of their final *cp* phases is larger than that of their initial *op* counterparts. These results indicate that the dense phase is a temporary state, while the *cp* phase is metastable. Fig. 3(c) and Fig S1(c) show the atomic structures of these three phases of five DUT materials, which are extracted from the trajectory files in MD simulations. Specifically, *op*, *cp* and dense phases are, respectively, obtained at the stages after the initial relaxtion (*t* = 1 ns), during the loading process (*t* = 6 ns) and after the unloading process (*t* = 12 ns). The most distinctive feature among the three phases is their porosity distribution (see Fig S3). The *op* phase exhibits a porous structure, while a nearly zero porosity is found in the dense phase. As the intermediate stage between *op* and dense phases, the *cp* phase has a medium porosity [7]. For convenience, in what follows, the dense phase is named as no pore (*np*) phase. This phase transition process leads to the loss of crystallinity, which is similar to the pressure-induced amorphization (PIA) process widely observed in various MOF crystals [5,48–51].

Supplementary video related to this article can be found at <https://doi.org/10.1016/j.micromeso.2020.110765>

As represented in Fig. 3(a) and Fig S1, the *op*→*cp* phase transition (marked by solid arrows) is observed in all considered DUTs. This initial *op*→*cp* phase transition is accompanied with a sharp volume contraction, which corresponds to the mechanical instability occurring in all DUTs. If we keep compressing the DUTs within the *cp* phase, different phenomena are observed in different DUTs. One direct transition process (marked by dotted arrows) is observed during the *op*→*cp* phase transition in DUT-48, -50, and -151. Although similar *op*→*cp* phase transition is also observed in DUT-49, this process includes two stages. As for DUT-46, no *op*→*cp* phase transition is observed, which means that the atomic structure of DUT-46 shrinks gradually and continuously after the initial *op*→*cp* phase transition.

Inspired by the previous studies on the NGA of DUT49,[39] in Fig. 3(b) and Fig S1(b) we show the local deflection of ligand backbones in all DUTs considered here, which is helpful for better understanding the microscopic mechanism of the mechanical instability occurring in DUTs under compression. Here, ligand backbones of different DUT materials are, respectively, noted as L₁ to L₅ shown in Fig. 2(b). As plotted in Fig. 3(b) and Fig S1(b), no significant deflection is found in the ligand backbone at the beginning, which corresponds to the elastic deformation of DUT materials without any topological changes. When the applied pressure is larger than a critical value, a large deflection suddenly occurs

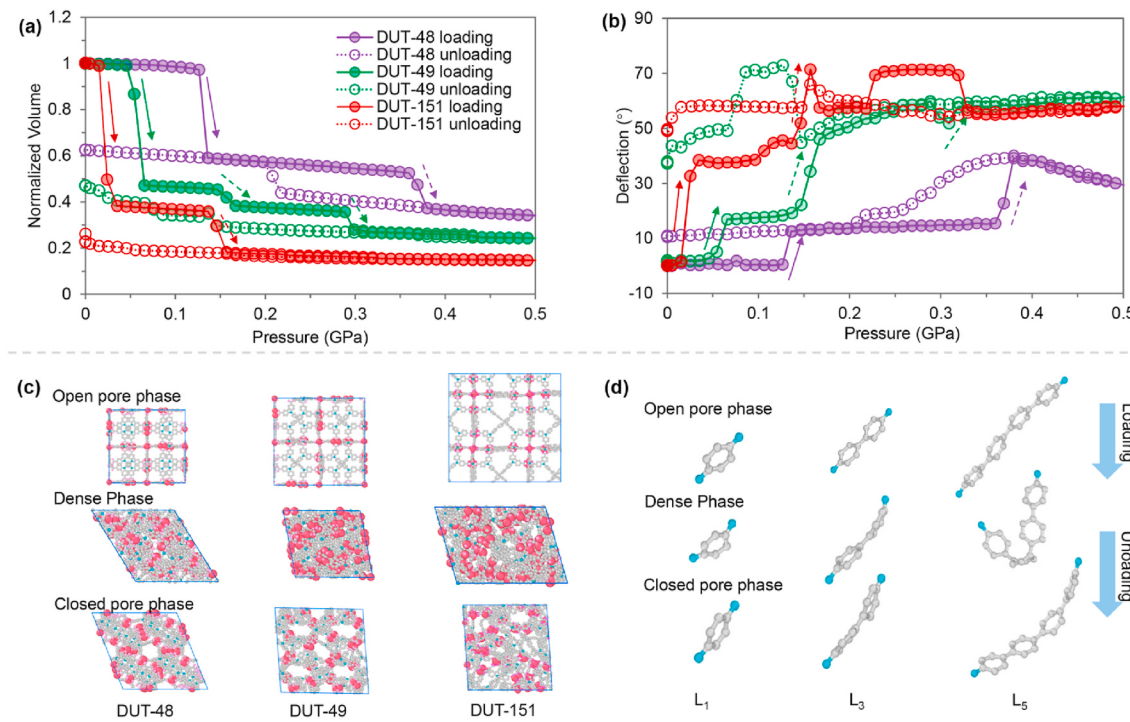


Fig. 3. Evolutions of (a) the normalized volume, (b) the deflection of ligand backbone, (c) the crystal structure, and (d) the ligand backbone structure of DUT-48, DUT-49, and DUT-151 upon pressure (see Fig S1 in supplementary materials for results of DUT-46 and DUT-50). Here, the closed and open circles in (a) and (b) correspond to loading and unloading processes, respectively. The arrows in (a) refer to the instability point at the critical pressure. The deflection in (b) is measured by the N-centroid-N angle. The snapshots of open and closed pore phases in (c) are extracted from the molecular simulations at the initial relaxation stage and the final stage after the entire loading and unloading processes.

in ligands (see the solid arrows), which denotes the occurrence of buckling instability in ligands. The critical buckling pressure of ligands is identical to the critical pressure triggering the mechanical instability of DUT materials. This agreement reveals that the buckling of ligands accounts for the global phase transition occurring in DUTs after they lose the mechanical stability. With increasing pressure, the ligands undergo larger buckling deformations, which result in the further phase transition of DUT materials from the *cp* phase to the *np* phase (see the dotted arrows). After the pressure is completely released, deflections can retain in ligands, which denotes that the DUT materials can no longer recover to their initial *op* phases. Moreover, a larger buckling deformation is observed in longer ligands during both the loading and unloading processes, which indicates more significant volume contraction occurring in DUTs with longer ligands as shown in Fig. 3 and Fig S1(a).

Although all five isoreticular DUT materials have the similar phase transition feature in real-time MD simulations, the critical pressures of phase transition are different for different DUT materials. The critical pressures of *op*–*cp* phase transition and *cp*–*np* phase transition of DUT materials obtained from real-time MD simulations are shown in Table 2 and Fig S4, respectively. It is worth mentioning that because we mainly focus on the mechanical instability of DUT materials corresponding to the first phase transition observed, the critical pressure of the first *op*–*cp*.

Table 2
The critical pressure accounting for mechanical instability of isoreticular DUT materials.

DUT crystals	P_{cr} (MPa)		
	Real-time MD	<i>P</i> – <i>V</i> EOS	Born stability criteria
DUT-48	125.8	138.8	145.4
DUT-46	88.3	81.4	67.7
DUT-49	57.0	59.6	55.1
DUT-150	31.6	35.2	30.3
DUT-151	21.1	21.3	19.9

phase transition will be mainly discussed in the rest part of this paper.

(ii) Born stability criteria

To understand the mechanical instability of isoreticular DUT crystals from the global viewpoint, we investigate the evolution of the Born criteria when the pressure grows from -200 MPa to the value corresponding to the failure of materials. Here, all material parameters involved in the Born criteria are calculated from the strain fluctuation method [52], which include elastic constants (C_{11} , C_{12} and C_{44}), elastic moduli (bulk, Young's and shear modulus), Poisson's ratio, and the anisotropy in Young's and Shear modulus. The maximum and minimum Young's moduli of DUT materials are observed in the crystal axis and body diagonal, respectively, since DUT materials possess the smallest and largest porosity in the diagonal direction and the crystal axis, respectively. In contrast, the shear modulus has the maximum value and the minimum value along the crystal axis and body diagonal direction, respectively (see Fig S5). As expected, the elastic moduli including Young's, bulk, and shear modulus of DUTs shown in Fig. 4(a) follow the order of DUT-48, -46, -49, -50 and -151, since the elastic moduli decrease as the porosity of DUT materials increases.

According to Eq (1), the critical transition pressure corresponds to the smallest extrapolated value among three independent Born stability criteria, which represent three instability deformation modes. Fig. 4(b) shows the evolution of Born stability criteria of five DUTs with increasing pressure. As for DUT-48 and DUT-151, C_{44} –*P* is found to be the primary criterion determining the phase transition, which indicates that the mechanical instability occurs in a shear deformation mode. However, as for other DUT materials such as DUT-46, DUT-49 and DUT-50, the isotropic tensile deformation is responsible for the mechanical instability, because in these three materials C_{11} – C_{12} –2*P* turns to be the primary criterion.

As predicted from Fig. 4, the critical transition pressures of DUT-48,

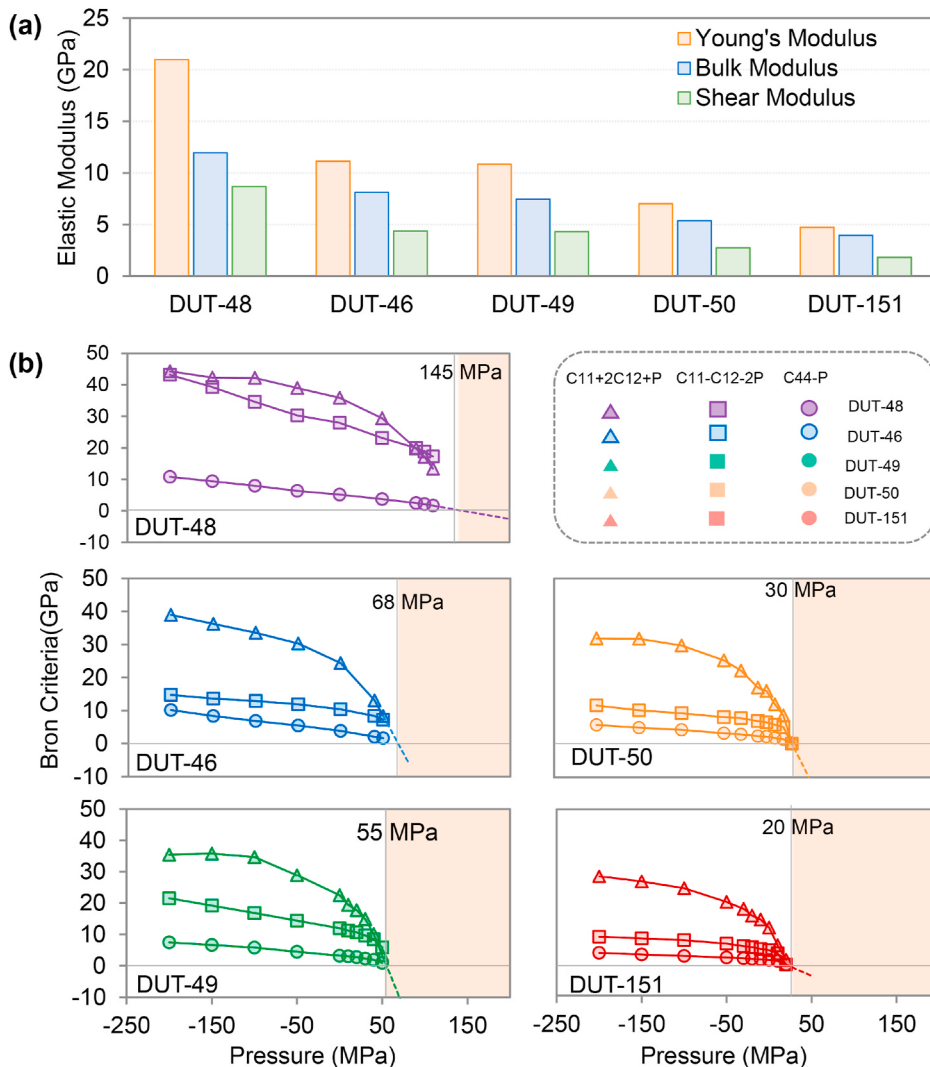


Fig. 4. (a) The bulk modulus, Young's modulus and shear modulus of five DUT materials at 0 GPa. (b) Born stability criteria of five DUT materials as a function of the applied pressure at 300 K. The triangle, square and circle symbols refer to three independent criteria, i.e., resistance to hydrostatic loading, to tensile loading with conserved volume in first order, and to the shear loading. The dotted line is an extension of the linear fitting of two closest data points. The critical pressure of instability is predicted as the intersect point between zero horizon and dotted line.

-46, -49, -50, and -151 are 145 MPa, 68 MPa, 55 MPa, 30 MPa, and 20 MPa, respectively. Expect DUT-46, the critical transition pressures of other DUT materials predicted from the Born criteria are very close to the results obtained by real-time MD simulations shown in Fig. 7. The difference between two methods observed in DUT-46 can be attributed to the fact that the results obtained near the instability region are not reliable due to numerical errors. As suggested by Rogge et al. [37], the instability pressure (responsible for PIT or PIA) of flexible MOFs such as MIL-53(Al) [34], COMOC-2,[53] and DUT-49[39] is usually less than 100 MPa, while the rigid MOFs including MOF-5,[22] Uio series (Uio-66, -67 and -68) [54], ZIF-4, and ZIF-8[49] can withstand a larger pressure. Based on this discrepancy, our calculations show that the isoreticular DUT materials with different ligands can shift from a rigid material (DUT48) to a flexible material (other DUT materials). The flexible/rigid features of DUT materials can also be detected from the changes in their mechanical properties including bulk, Young's and shear modulus as plotted in Fig. 4(a), since the elastic moduli of isoreticular DUT materials generally decrease with increasing link length resulting in the increase of porosity of isoreticular DUT materials.

(iii) Anisotropy in elastic moduli

Anisotropy of mechanical properties shown in Fig. 1(c) is another widely used flexible/rigid criterion for MOF crystals. Thus, in what follows, we examine the evolution of the anisotropy in the elastic

properties of isoreticular DUT materials when they shift from rigid materials to flexible materials with increasing organic linker length. Fig. 5(a) shows the anisotropy in Young's and shear moduli of DUT materials upon different pressures. The yield anisotropy factors of all DUT materials are less than 4.0, which is in contrast to the value larger than 100 previously suggested for flexible crystals as shown in Fig. 1(c) [33]. The anisotropy in Young's and shear moduli shows the similar relation with the applied pressure. The anisotropy in both elastic moduli is found to grow gently as the pressure grows at the initial stage. When approaching the instability region, a great increase is found in the anisotropy in Young's and shear moduli for all DUT materials except DUT-50, whose anisotropy in Young's and shear moduli experiences a sudden drop.

It is found that the mechanical anisotropy of flexible DUT materials calculated in this study (<4.0) is much smaller than 100. The present result is similar with the value of rigid Uio-66 (1.2)[27, 37] and ZIF-8 (1.4) [33,55], but is in contrast to the values of some other flexible MOF crystals such as MIL-53(Al) (105), MIL-53(Ga) (444), and MIL-47 (108) [33]. The exception of DUT materials in our study suggests that the high anisotropy ratio (>100) of an MOF crystal can be used to determine its flexible property, but the anisotropy factor of a flexible MOF is not necessary to be larger than 100.

Considering three representative pressure states (-200 MPa, 0 MPa, and the critical pressure near the instability region), in Fig. 5(b) we show the spatial dependence of Young's and shear moduli, which are,

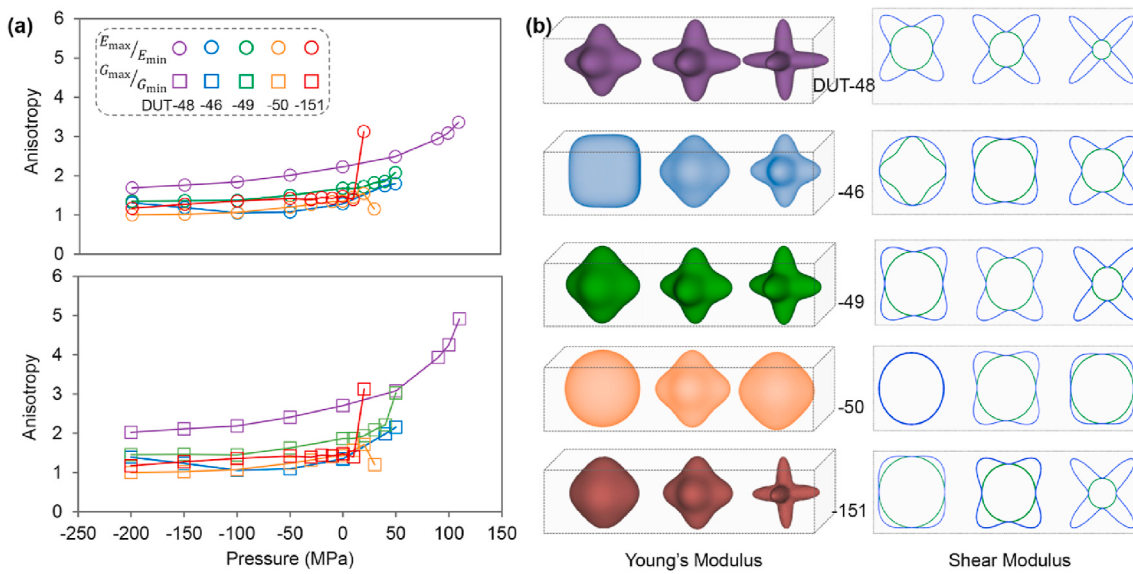


Fig. 5. (a) The evolution of anisotropy in Young's and shear moduli of five DUT materials upon pressure. (b) Spatial dependence of Young's modulus (left, represented in 3D spherical coordinates) and shear modulus (right, represented in 2D plane coordinates) of five DUT materials under three different loading states: -200 MPa, 0 MPa, and the critical pressure close to the instability region. Here, the spatial values are normalized by their corresponding maximum values.

(iv) Pressure-versus-volume equations of state

respectively, depicted in 3D spherical and 2D plane coordinates. Interestingly, it is found that DUTs materials under some certain pressures can transform from anisotropic materials to isotropic materials. For example, DUT-46, DUT-50, and DUT-151 under -200 MPa and DUT-50 under 30 MPa are found to possess isotropic elastic properties.

In Ref. [6], Krause et al. investigated the PIT in DUT serials from the view of free energy by calculating P - V EOS. Inspired by this work, we adopt a similar approach to obtain P - V EOS of five DUT materials, which provides thermodynamics insights into the phase transitions of DUTs.

Fig. 6(a) and (b), respectively, show the pressure and free energy of DUT-49 with different volumes. Here, the free energy was obtained from Eq S(7) in supplementary materials. The corresponding results of other

DUT materials are shown in Fig S6 and S7 in the supplementary materials. According to Eq S(6), the critical transition pressure P_{cr} is the local maximum of pressure, at which the slope of the pressure-volume curve in Fig. 6(a) transforms from negative to positive. The critical transition pressure of five DUT materials obtained from P - V EOS method is summarized in Table 2, in which the results obtained from real-time MD simulations and Born stability criteria are also shown for the sake of comparison. The critical transition pressures obtained by these three methods are very close to each other, especially for the most flexible DUT-151 crystal. It was suggested in the previous study [34] that due to the pressure fluctuations, real-time MD simulations may lead to a great underestimation of the critical transition pressure. However, the

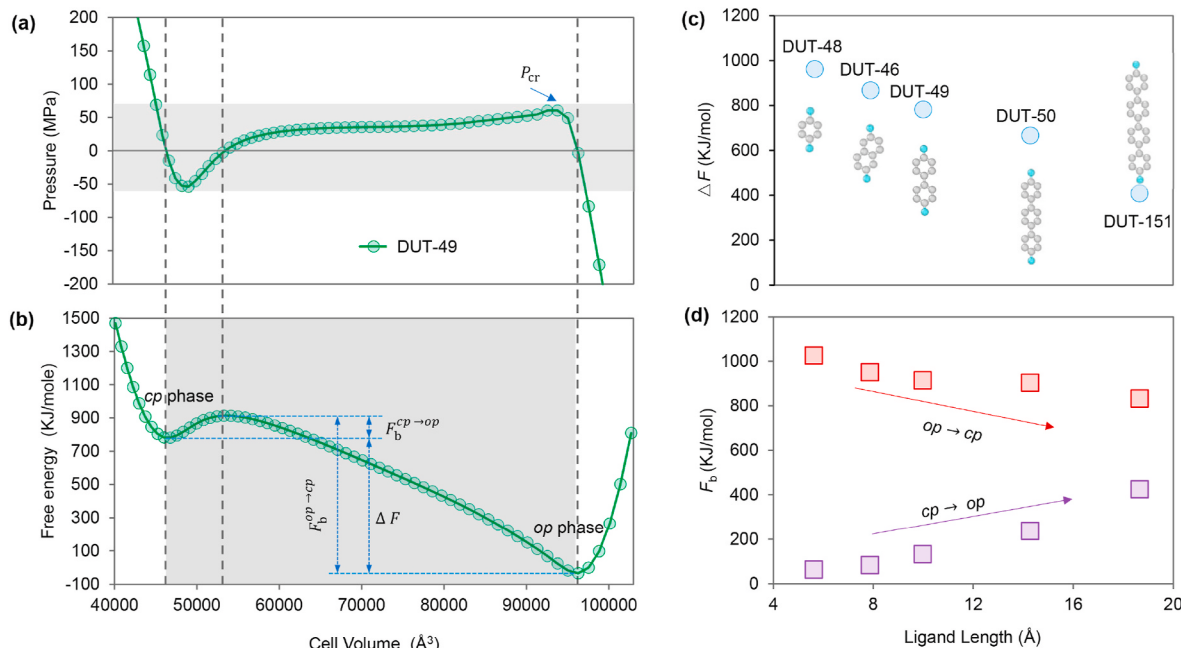


Fig. 6. (a) P - V EOS and (b) corresponding free energy of DUT-49 crystal. (c) Free energy difference between *op* and *cp* phases of different DUT materials as a function of the ligand length. (d) Energy barrier of *op* to *cp* and inverse *cp* to *op* transition as a function of the ligand length.

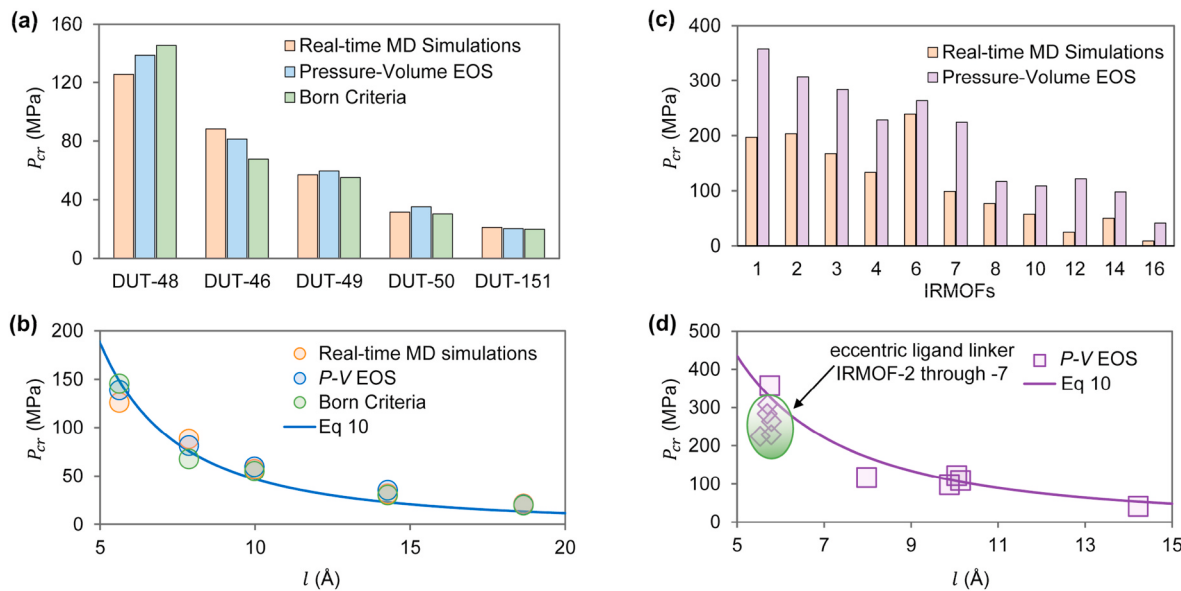


Fig. 7. (a) The critical transition pressure P_{cr} of DUTs obtained from real-time MD simulations, P - V EOS method, and Born stability criteria. (b) The relationship between P_{cr} of DUTs and their ligand length l , which is calculated from three computational approaches and also predicted from the mechanical model, i.e., Eq (9). (c) The critical transition pressure P_{cr} of IRMOFs obtained from real-time MD simulations and P - V EOS method. (d) The relationship between P_{cr} of IRMOFs and their ligand length l , which is calculated from P - V EOS method and also predicted from the mechanical model. Here, IRMOFs with straight ligand linker, i.e., IRMOF-1, -8, -10, -12, -14, and -16, are adopted for the curve fitting.

underestimation of critical transition pressure does not exist in the present real-time MD simulations. We even find the critical transition pressure of DUT-46 calculated by real-time MD simulations is significantly larger than the result extracted from EOS method. In other isoreticular MOF series such as IRMOFs, which will be discussed in detail later, a large underestimation of the critical transition pressure is found in real-time MD simulations.

The free energy, as shown in Fig. 6(b), is obtained by integrating the results in Fig. 6(a) by the trapezoidal rule. Here, the original op phase is set as the base point. Three zero points of pressure in Fig. 6(a) from right to left, respectively, represent the state of original op phase, the barrier of $op \rightarrow cp$ transition, and the metastable cp phase. The simple relationship among the free energies at different states can be written as:

$$F_b^{op \rightarrow cp} = \Delta F + F_b^{cp \rightarrow op} \quad (4)$$

where ΔF is the free energy difference between the transformed cp phase and the original op phase, $F_b^{op \rightarrow cp}$ is the energy barrier of the $op \rightarrow cp$ transition, and $F_b^{cp \rightarrow op}$ denotes the energy barrier of the inverse $cp \rightarrow op$ transition. The specific values of free energy at different states in five DUT materials are graphically shown in Fig. 6(c) and (d). All values of ΔF are positive, indicating that the cp phases of all DUT materials are metastable. This result is in good agreement with the result obtained from the above real-time MD simulations. ΔF of isoreticular DUT series significantly declines from 961.8 kJ/mol to 408.0 kJ/mol when the ligand length is extended from 5.6 Å (DUT-48) to 18.7 Å (DUT-151). A similar relation is also found between the energy barrier $F_b^{op \rightarrow cp}$ and the ligand length, since $F_b^{op \rightarrow cp}$ is found to almost linearly decrease with increasing ligand length. However, the energy barrier $F_b^{cp \rightarrow op}$ shows an opposite relation with the ligand length, which increases as the ligand length increases. These results indicate that the isoreticular DUT materials with longer ligand possess a more stable cp phase, which are easier to experience the $op \rightarrow cp$ transition and thus are more difficult to recover from the cp phase. As described in above real-time MD simulations and previous studies [7,39], the global instability occurring in DUT materials originates from the local buckling of their ligand. The Euler buckling law indicates that the critical buckling force of a column is inversely proportional to the square of the length [56]. Accordingly, a longer

ligand requires a smaller force (and corresponding a smaller work) to drive the global instability, which can well explain the smaller ΔF and $F_b^{op \rightarrow cp}$ observed in isoreticular DUT materials with a longer ligand (see Fig. 6(c) and (d)).

The bulk modulus K can be estimated from the P - V curves shown in Fig. 6(b):

$$K = -V \frac{\partial P}{\partial V} \quad (5)$$

Based on Eq (5), we calculate the bulk modulus of op and cp phases, which is implemented by applying the linear fitting to the data near the equilibrium state. The obtained results are shown in Fig S8. For the sake of comparison, the bulk modulus of op phase of isoreticular DUT series obtained by the above strain-fluctuation method is also shown here (see Eq S(2) and Fig. 5(b)). It is found that the bulk Young's modulus extracted from these two methods have the similar relation with the ligand length, which decreases as the ligand length grows. However, the magnitude of the bulk Young's modulus calculated by the EOS method is slightly smaller than the result obtained by the strain-fluctuation method. This difference mainly can be attributed to the fact that only limited discrete points are available in the EOS method. In addition, the bulk modulus of DUT materials within the cp phase is found to be only ~2.0 GPa, which is much lower than the value 3.7–8.2 GPa of their counterparts within the op phase. This fact indicates that the cp phase of DUT materials has the weak ability to resist isotropic compression deformation, which thus is easy to transform into the np phase under hydrostatic pressure.

Based on molecular simulations, in this section we have conducted a comparative study of four different computational approaches in dealing with the phase transition occurring in isoreticular DUT materials under compression. In summary, real-time MD simulations indicate that PIT is caused by the buckling of ligands; the Born stability criteria prove that the mechanical instability of DUT materials is dominated by shear and isotropic tensile deformation modes; the anisotropy factor of flexible DUT crystals is found to be in the range of 0–5, which is in contrast to the value larger than 100 suggested in the previous theory [33]; the P - V EOS method presents a thermodynamic insight into the mechanism of the ligand-dependent instability of isoreticular DUT materials.

3.2. Ligand-dependent critical transition pressure of DUTs and IRMOFs

As plotted Fig. 7(a), we compare the critical transition pressures P_{cr} of isoreticular DUT materials obtained from three different methods including real-time MD simulations, P - V EOS method, and Born stability criteria. Results obtained from these three methods are found to be identical to each other. Specifically, the obtained results show that P_{cr} decreases with increasing ligand length l , which indicates that the mechanical instability is easier to occur in isoreticular DUT materials with a longer ligand. To figure out whether the relation between P_{cr} and l extracted from the present isoreticular DUT materials is general for other isoreticular MOF crystals, we investigate another isoreticular MOF series, i.e., the classical IRMOFs. Similar to DUTs, IRMOFs are also cubic materials. The only difference between these two materials is that the metal group of oxide-centered Zn_4O in IRMOFs is edge-bridged by six ligand linkers of carboxylates as shown in Fig. 2(b), while in DUTs each 12-connective cuboctahedral building block is bridged by twelve ligand backbones as shown in Fig. 2(a). This structural difference is analogous to the difference between a simple-cube crystal and a face-centered-cube crystal (see Fig S9). All IRMOFs can be divided into two groups based on whether the centroid of ligand deviates from the center line connected to the second build units: one is with straight ligand and the other is with eccentric ligand. Accordingly, IRMOF-2 through -7 are IRMOFs with eccentric ligand, while others are IRMOFs with straight ligand.

Both real-time MD simulations and P - V EOS method are used to estimate the critical transition pressure of IRMOF series. The obtained results are shown in Fig. 7(c) and also are listed in Table S2. Here, the calculation methods are exactly the same as the those previously adopted for DUTs. P_{cr} obtained from both methods shows the similar relation with the ligand length, which decreases with increasing ligand length. However, a significant gap is still detected between the values obtained from these two methods. Especially for the flexible IRMOFs such as IRMOF-12 and IRMOF-16, the ratio of result obtained from EOS method to that extracted from real-time MD simulations can even be up to ~ 4.8 . This difference is probably caused by the characteristics of the UFF force field. Compared to the state of art first-principle derived MOF-FF force field, the present UFF4MOF force field is less accurate to describe dynamic properties in real-time MD simulations, because it can cause serious pressure fluctuations [57]. However, in EOS calculations each simulation is conducted in the thermodynamic ensemble with the fixed volume [34,37,58], which, to some extent, can mitigate the effect of pressure fluctuations. As a result, EOS method provides more accurate results compared to those directly from real-time MD simulations. Under this circumstance, P_{cr} extracted from EOS method is selected as the estimated critical transition pressure in the following discussion.

Fig. 7(d) shows the critical transition pressure P_{cr} of IRMOF crystals with different ligand lengths l . A relation between P_{cr} and l similar to the result observed in above DUT series is found in IRMOF crystals with straight ligand, i.e., IRMOF-1 and -8 through -16. However, the critical transition pressure P_{cr} of IRMOFs with eccentric ligand, i.e., IRMOF-2 through -7, is quite lower than that of IRMOF-1 (with straight ligand), though they almost have the same ligand length. As plotted in Fig S11, the centroid line of IRMOF-2 through -7 is deviated from the centerline of the compressive force, which thus equivalently induces an additional bending moment on these IRMOFs. This additional bending moment makes IRMOF-2 through -7 easier to lose stability, which is responsible for lower critical transition pressure observed in them. A similar mechanism was also reported very recently for Uio series, whose distorted linkers are responsible for their small bulk modulus [59].

Based on the above results of two isoreticular MOF series, i.e., DUTs and IRMOFs, we can conclude that the PIT behavior of DUT materials is dependent heavily on their ligand, especially the length of ligand. It is noted that although the above computational approaches can be applied to determine the stability of MOFs from different aspects, they all have their own limitations. Real-time MD simulations may underestimate the hydrostatic pressure in some cases; the evolution of Born stability

criteria may exhibit strong nonlinearity when approaching the instability region; the theory of anisotropy in elastic moduli is inaccurate in calculating the instability pressure as it fails to predict the flexible/rigid property of DUTs; the P - V EOS method relies on a large number of discrete points, each of which needs long time relaxation and sampling. In addition, the aforementioned computational approaches cannot automatically reveal the physics behind the observed behaviors, especially the ligand-dependent critical transition pressure of isoreticular MOFs. Under these circumstances, it becomes crucial to construct a reliable analytic model to predict the stability of MOF crystals under compression. As an initial attempt, in what follows, we develop a preliminary mechanical model for isoreticular MOFs. This model is not only helpful for understanding the nature of the mechanical instability occurring in isoreticular MOFs, but also can be utilized to give a quick estimation of the critical transition pressure of isoreticular MOFs.

3.3. A mechanical model to predict the critical transition pressure of isoreticular MOFs

As mentioned above, the instability of isoreticular MOF crystals is driven by the local buckling of their ligand backbones. Herein, the Euler buckling law as shown in Fig. 1(e) is introduced to describe the buckling of ligand linkers, which is usually employed to calculate the critical buckling force of a slender column and to predict the out-of-plane buckling behaviors of thin films such as 2D covalent organic framework [60].

Considering the fact that the ligand backbone can be equivalently treated as a slender column, the buckling of ligand backbone thus obeys the Euler buckling law $f_{cr} = \beta_1 EI/l^2$, where f_{cr} is the critical buckling force, E is the equivalent elastic modulus, I is the second moment of area, and β_1 is a structural parameter depending on the boundary conditions. After treating the ligand backbone as a column with length l , width b and thickness h (as depicted in Fig S12), I can be written as $bh^3/12$. Then, the Euler buckling law can be rewritten as

$$f_{cr} = \frac{\beta_1 Ebh^3}{12l^2} \quad (6)$$

As the ligand has a single-chain structure, it is difficult to define its cross-sectional area S . Thus, we define the elastic modulus E_f here as $E_f = ES = Ebh$, which has a unit of nN. Then, Eq (6) can be further simplified into

$$f_{cr} = \frac{\beta_2 E_f}{l^2} \quad (7)$$

where $\beta_2 = \beta_1 h^2/12$. It is reasonable to assume that the ligands in isoreticular MOFs in one series have the same thickness, since they all share a single atomic layer in the thickness direction. Thus, β_2 is a constant for the same series of isoreticular MOFs. This assumption can be verified by Fig. 8(a), which shows that the previously calculated results of f_{cr} can be well fitted by Eq (7).

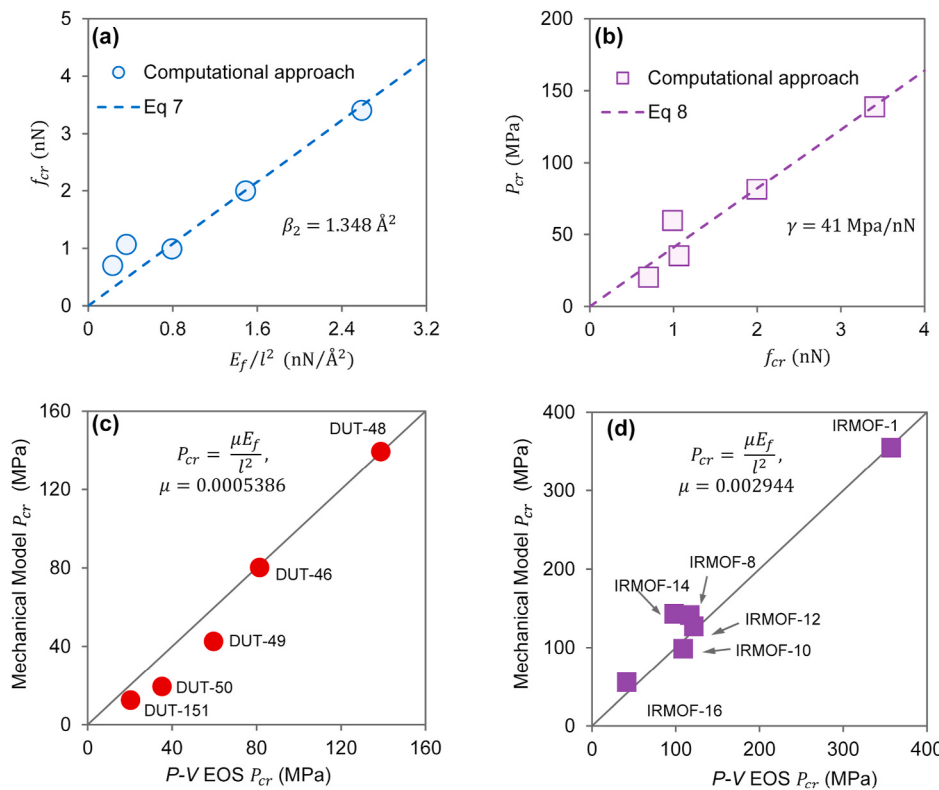
In addition, as shown in Fig. 8(b), the critical transition pressure of isoreticular MOFs is almost proportional to the critical buckling force of their ligand, which results in the following linear relation between P_{cr} and f_{cr} :

$$P_{cr} = \gamma f_{cr} \quad (8)$$

where γ is a scale factor related to the crystal structure of MOFs. Substituting Eq 7 into 6, we obtain the following expression of P_{cr} :

$$P_{cr} = \frac{\mu E_f}{l^2} \quad (9)$$

Here, $\mu = \beta_2/\gamma$ is a dimensionless topology parameter related to structural topology of isoreticular MOFs. Thus, Eq (9) implies that the stability of isoreticular MOF crystals is generally determined by three parameters: the topology parameter μ , the elastic modulus of ligand E_f ,



and the ligand length l . The value of μ can be easily obtained by fitting Eq. (9) to the results extracted from the above computational approaches, which equals to 0.0005386 and 0.002944 for DUTs and IRMOFs, respectively.

Next, we apply the mechanical model of Eq (9) to predict the critical transition pressure P_{cr} of both DUTs and IRMOFs. It should be noted that IRMOFs with eccentric ligand, i.e., IRMOF-2 through -7 are not considered here. As shown in Fig. 8(c) and (d), the critical transition pressure P_{cr} predicted from the present mechanical model is identical to the result extracted from $P\text{-V EOS}$ method. In addition to the results obtained from the computational method, as shown in Fig S14, the results of DUTs measured from experiments [6] also can be fitted by the proposed mechanical model though the fitting parameter μ is slightly smaller than that from above simulation results. This difference can be attributed to the fact the Hg intrusion in experiments can possibly lead to additional pressure in isoreticular MOFs [6,61], which can cause bond breakage and thus accelerate the occurrence of transition. These facts indicate that our mechanical model is reliable and accurate in estimating the critical transition pressure for both DUT and IRMOF series. On the other hand, our mechanical model also has some limitations, which thus needs further improvement. For example, in terms of some IRMOF crystals such as IRMOF-8 and IRMOF-14, the difference between the mechanical model and $P\text{-V EOS}$ method can be larger than 20% (see Fig S15). This significant difference might originate from the fact that some nonbonding effects such as the van der Waals and Coulombic interactions cannot be included in the mechanical model. Moreover, our mechanical model is based on the assumption that the mechanical instability of isoreticular MOFs is totally induced by the buckling of their ligand backbone; however, some factors such as shear modulus softening [19,27,49], node-linker bond effect [16,25,62], and configurational (or vibrational) entropic effect [35,36] may also contribute to the mechanical instability of isoreticular MOFs, which are ignored in the present mechanical model for simplicity.

According to Eq (9), when compared to other two parameters μ and E_f , the ligand length l has a more profound impact on the flexible/rigid

Fig. 8. (a) The relationship between f_{cr} and E_f/l^2 in Eq (7). (b) The relationship between f_{cr} and P_{cr} in Eq (8). Here, the ligand length l and critical transition pressure P_{cr} are listed in Tables 1 and 2, respectively. Values of critical load f_{cr} and elastic modulus E_f of ligand linkers are obtained from first-principles calculations in Ref. 6 (these specific values are listed in Table S3). The comparison of the critical transition pressure of isoreticular (c) DUTs and (d) IRMOFs calculated from $P\text{-V EOS}$ method and estimated by the mechanical model. Here, elastic moduli of six IRMOF materials are obtained by first-principle calculations as shown in Fig S13.

property of isoreticular MOFs. A similar strategy by changing the ligand length has been previously adopted in chemical synthesis and experiments to achieve the NGA transitions in isoreticular DUT materials [6]. Another good strategy to control the flexible/rigid property of MOF crystals is to change the elastic modulus, i.e., the stiffness of ligand linker. Very recently, Krause et al. [63] developed a novel DUT series by softening the ligand backbone via the incorporation of sp [3] hybridized carbon atoms. Specifically, among these new DUT series, the new DUT-160 is found to possess the largest NGA ever observed [63]. As for one series of isoreticular MOF crystals, the elastic modulus E_f could be reasonably assumed to keep unchanged. Thus, our mechanical model can be further simplified into an equation that only depends on a single parameter l :

$$P_{cr} = a/l \quad (10)$$

Here $a = \mu E_f$, which can be regarded as a constant parameter for MOF crystals in one isoreticular series. As plotted in Fig. 7(b) and (d), the results of critical transition pressure of both DUTs and IRMOFs extracted from the computationally expensive $P\text{-V EOS}$ method can be well fitted by Eq (10), which indicates that this simple model can be utilized to give a quick estimation of the critical transition pressure of isoreticular MOFs.

4. Conclusions

In this paper, PIT of isoreticular DUT materials is investigated by four computational approaches at the molecular scale, which include real-time MD simulations, Born stability criteria, the anisotropy in elastic moduli, and the $P\text{-V EOS}$ method. The results extracted from different methods shed lights on the nature and mechanism of the stability of MOF crystals from different aspects. Moreover, the critical transition pressures calculated from real-time MD simulations, Born stability criteria, and $P\text{-V EOS}$ method are found to be identical to each other, which indicates their reliability in determining the mechanical instability of isoreticular DUT materials. However, the approach of

anisotropy in elastic moduli fails to evaluate the flexible/rigid property of isoreticular DUT crystals, since the rigid feature of isoreticular DUT crystals determined from the anisotropy of their elastic moduli is in conflict with the low critical transition pressures obtained from the previous computational approaches.

Our computational studies also reveal that the global instability of MOF crystals is driven by the local buckling of their ligands. Based on this finding, we develop a simple mechanical model to predict the critical transition pressure of isoreticular MOF materials, which only contains three parameters including the topology constant, the elastic modulus of ligand and the ligand length. It is found that our mechanical model can reliably describe the transition pressure of various isoreticular MOF materials such as DUT and IRMOF materials. In addition, our mechanical model also provides a design criterion for isoreticular MOF crystals to modify their rigid/flexible properties by changing the aforementioned three parameters. Actually, similar ligand- and elastic modulus-dependent critical transition pressure have been successfully employed in the very recent experiments of isoreticular DUT crystals [6, 63]. Overall, this work not only provides molecular insights into the ligand- and pressure-dependent mechanical behaviors of isoreticular MOFs, but also offers a predictive equation for quickly predicting the mechanical stability of isoreticular MOFs.

CRediT authorship contribution statement

Penghua Ying: Conceptualization, Methodology, Investigation, Formal analysis, Writing - original draft, Writing - review & editing. **Jin Zhang:** Conceptualization, Formal analysis, Writing - review & editing. **Zheng Zhong:** Resources, Writing - review & editing, Supervision, Project administration, Funding acquisition.

Declaration of competing interest

The authors declare that they have no known competing financial interests or personal relationships that could have appeared to influence the work reported in this paper.

Acknowledgements

This study was supported by the National Key R&D Program of China (no. 2018YFB1502600) and the National Natural Science Foundation of China (nos. 11932005, 11772106, and 11602074).

Appendix A. Supplementary data

Supplementary data related to this article can be found at <https://doi.org/10.1016/j.micromeso.2020.110765>.

References

- [1] J.K. Mohamed Eddaoudi, Nathaniel Rosi, David Vodak, Joseph Wachter, Michael O'Keeffe, Omar M. Yaghi, Systematic design of pore size and functionality in isoreticular MOFs and their application in methane storage, *Science* 295 (2002) 469–472.
- [2] O.M. Yaghi, M. O'Keeffe, N.W. Ockwig, H.K. Chae, M. Eddaoudi, J. Kim, Reticular synthesis and the design of new materials, *Nature* 423 (6941) (2003) 705–714.
- [3] G. Chaplaïs, G. Fraux, J.-L. Paillaud, C. Marichal, H. Nouali, A.H. Fuchs, F.-X. Coudert, J. Patarin, Impacts of the imidazolate linker substitution (CH_3 , Cl , or Br) on the structural and adsorptive properties of ZIF-8, *J. Phys. Chem. C* 122 (47) (2018) 26945–26955.
- [4] B. Mortada, G. Chaplaïs, V. Veremeienko, H. Nouali, C. Marichal, J. Patarin, Energetic performances of ZIF-8 derivatives: impact of the substitution (me, Cl, or Br) on imidazolate linker, *J. Phys. Chem. C* 122 (7) (2018) 3846–3855.
- [5] P. Ying, J. Zhang, X. Zhang, Z. Zhong, Impacts of the functional group substitution and pressure on the thermal conductivity of ZIF-8, *J. Phys. Chem. C* 124 (11) (2020) 6274–6283.
- [6] S. Krause, J.D. Evans, V. Bon, I. Senkovska, P. Iacomi, F. Kolbe, S. Ehrling, E. Troschke, J. Getzschmann, D.M. Tobbens, A. Franz, D. Wallacher, P.G. Yot, G. Maurin, E. Brunner, P.L. Llewellyn, F.X. Coudert, S. Kaskel, Towards general network architecture design criteria for negative gas adsorption transitions in ultraporous frameworks, *Nat. Commun.* 10 (1) (2019) 3632.
- [7] S. Krause, V. Bon, I. Senkovska, U. Stoeck, D. Wallacher, D.M. Többens, S. Zander, R.S. Pillai, G. Maurin, F.-X. Coudert, S. Kaskel, A pressure-amplifying framework material with negative gas adsorption transitions, *Nature* 532 (7599) (2016) 348–352.
- [8] V. Guillerm, F. Ragon, M. Dan-Hardi, T. Devic, M. Vishnuvarthan, B. Campo, A. Vimont, G. Clet, Q. Yang, G. Maurin, G. Ferey, A. Vittadini, S. Gross, C. Serre, A series of isoreticular, highly stable, porous zirconium oxide based metal-organic frameworks, *Angew. Chem. Int. Ed. Engl.* 51 (37) (2012) 9267–9271.
- [9] B. Van de Voorde, D. Damasceno Borges, F. Vermoortele, R. Wouters, B. Bozbiyi, J. Denayer, F. Taulelle, C. Martineau, C. Serre, G. Maurin, D. De Vos, Isolation of renewable phenolics by adsorption on ultrastable hydrophobic MIL-140 metal-organic frameworks, *ChemSusChem* 8 (18) (2015) 3159–3166.
- [10] L.R. Redfern, L. Robison, M.C. Wasson, S. Goswami, J. Lyu, T. Islamoglu, K. W. Chapman, O.K. Farha, Porosity dependence of compression and lattice rigidity in metal-organic framework series, *J. Am. Chem. Soc.* 141 (10) (2019) 4365–4371.
- [11] N.C. Burtch, J. Heinen, T.D. Bennett, D. Dubbeldam, M.D. Allendorf, Mechanical properties in metal-organic frameworks: emerging opportunities and challenges for device functionality and technological applications, *Adv. Mater.* 30 (37) (2018), e1704124.
- [12] P.Z. Moghadam, S.M.J. Rogge, A. Li, C.-M. Chow, J. Wieme, N. Moharrami, M. Aragues-Anglada, G. Conduit, D.A. Gomez-Gualdrón, V. Van Speybroeck, D. Fairén-Jiménez, Structure-mechanical stability relations of metal-organic frameworks via machine learning, *Matter* 1 (1) (2019) 219–234.
- [13] J.C. Tan, T.D. Bennett, A.K. Cheetham, Chemical structure, network topology, and porosity effects on the mechanical properties of Zeolitic Imidazolate Frameworks, *Proc. Natl. Acad. Sci. Unit. States Am.* 107 (22) (2010) 9938–9943.
- [14] T.D. Bennett, J. Sotelo, J.-C. Tan, S.A. Moggach, Mechanical properties of zeolitic metal-organic frameworks: mechanically flexible topologies and stabilization against structural collapse, *CrystEngComm* 17 (2) (2015) 286–289.
- [15] L.R. Redfern, O.K. Farha, Mechanical properties of metal-organic frameworks, *Chem. Sci.* 10 (46) (2019) 10666–10679.
- [16] L. Robison, R.J. Drout, L.R. Redfern, F.A. Son, M.C. Wasson, S. Goswami, Z. Chen, A. Olszewski, K.B. Idrees, T. Islamoglu, O.K. Farha, Designing porous materials to resist compression: mechanical reinforcement of a Zr-MOF with structural linkers, *Chem. Mater.* 32 (8) (2020) 3545–3552.
- [17] M. Rubio-Martinez, C. Avci-Camur, A.W. Thornton, I. Imaz, D. Maspoch, M.R. Hill, New synthetic routes towards MOF production at scale, *Chem. Soc. Rev.* 46 (11) (2017) 3453–3480.
- [18] S.C. McKellar, S.A. Moggach, Structural studies of metal-organic frameworks under high pressure, *Acta Crystallogr. Sect. Sect. B Struct. Sci. Cryst. Eng. Mater.* 71 (6) (2015) 587–607.
- [19] A.J. Howarth, Y. Liu, P. Li, Z. Li, T.C. Wang, J.T. Hupp, O.K. Farha, Chemical, thermal and mechanical stabilities of metal-organic frameworks, *Nature Reviews Materials* 1 (3) (2016).
- [20] T.D. Bennett, A.K. Cheetham, A.H. Fuchs, F.-X. Coudert, Interplay between defects, disorder and flexibility in metal-organic frameworks, *Nat. Chem.* 9 (1) (2016) 11–16.
- [21] Y. Hu, H. Kazemian, S. Rohani, Y. Huang, Y. Song, In situ high pressure study of ZIF-8 by FTIR spectroscopy, *Chem. Commun.* 47 (47) (2011) 12694–12696.
- [22] A.J. Graham, D.R. Allan, A. Muszkiewicz, C.A. Morrison, S.A. Moggach, The effect of high pressure on MOF-5: guest-induced modification of pore size and content at high pressure, *Angew. Chem. Int. Ed.* 50 (47) (2011) 11138–11141.
- [23] I.E. Collings, A.L. Goodwin, Metal-organic frameworks under pressure, *J. Appl. Phys.* 126 (18) (2019) 181101.
- [24] G. Lal, M. Derakhshanbeh, F. Akhtar, D.M. Spasuk, J.-B. Lin, M. Trifkovic, G.K. H. Shimizu, Mechanical properties of a metal-organic framework formed by covalent cross-linking of metal-organic polyhedra, *J. Am. Chem. Soc.* 141 (2) (2019) 1045–1053.
- [25] S.M.J. Rogge, P.G. Yot, J. Jacobsen, F. Muniz-Miranda, S. Vandenbrande, J. Gosch, V. Ortiz, I.E. Collings, S. Devautour-Vinot, G. Maurin, N. Stock, V. Van Speybroeck, Charting the metal-dependent high-pressure stability of bimetallic UiO-66 materials, *ACS Materials Letters* 2 (4) (2020) 438–445.
- [26] T.D. Bennett, A.K. Cheetham, Amorphous metal-organic frameworks, *Accounts Chem. Res.* 47 (5) (2014) 1555–1562.
- [27] H. Wu, T. Yildirim, W. Zhou, Exceptional mechanical stability of highly porous zirconium metal-organic framework UiO-66 and its important implications, *J. Phys. Chem. Lett.* 4 (6) (2013) 925–930.
- [28] T. Weng, J.R. Schmidt, Flexible and transferable ab initio force field for zeolitic imidazolate frameworks: ZIF-FF, *J. Phys. Chem. B* 123 (13) (2019) 3000–3012.
- [29] J. Heinen, D. Dubbeldam, On flexible force fields for metal-organic frameworks: recent developments and future prospects, *Wiley Interdiscipl. Rev. Comput. Mol. Sci.* 8 (4) (2018) e1363.
- [30] E.V. Alexandrov, A.V. Goltsev, R.A. Eremin, V.A. Blatov, Anisotropy of elastic properties of metal-organic frameworks and the breathing phenomenon, *J. Phys. Chem. C* 123 (40) (2019) 24651–24658.
- [31] G. Fraux, S. Chibani, F.-X. Coudert, Modelling of framework materials at multiple scales: current practices and open questions, *Phil. Trans. Math. Phys. Eng. Sci.* 377 (2149) (2019) 20180220.
- [32] M. Born, On the stability of crystal lattices. I, *Math. Proc. Camb. Phil. Soc.* 36 (2) (1940) 160–172.
- [33] A.U. Ortiz, A. Boutin, A.H. Fuchs, F.X. Coudert, Anisotropic elastic properties of flexible metal-organic frameworks: how soft are soft porous crystals? *Phys. Rev. Lett.* 109 (19) (2012) 195502.
- [34] S.M.J. Rogge, L. Vanduyfhuys, A. Ghysels, M. Waroquier, T. Verstraelen, G. Maurin, V. Van Speybroeck, A comparison of barostats for the mechanical

- characterization of metal–organic frameworks, *J. Chem. Theor. Comput.* 11 (12) (2015) 5583–5597.
- [35] L. Vanduyfhuys, S.M.J. Rogge, J. Wieme, S. Vandenbrande, G. Maurin, M. Waroquier, V. Van Speybroeck, Thermodynamic insight into stimuli-responsive behaviour of soft porous crystals, *Nat. Commun.* 9 (1) (2018) 204.
- [36] P. Vervoorts, J. Keupp, A. Schneemann, C.L. Hobday, D. Daisenberger, R. A. Fischer, R. Schmid, G. Kieslich, Configurational entropy driven high-pressure behaviour of a flexible metal–organic framework, *Angew. Chem. Int. Ed.* (2020), <https://doi.org/10.1002/anie.202011004>.
- [37] S.M.J. Rogge, M. Waroquier, V. Van Speybroeck, Reliably modeling the mechanical stability of rigid and flexible metal–organic frameworks, *Accounts Chem. Res.* 51 (1) (2018) 138–148.
- [38] S. Bureekaw, S. Amirjalayer, M. Tafipolsky, C. Spickermann, T.K. Roy, R. Schmid, MOF-FF - a flexible first-principles derived force field for metal–organic frameworks, *Phys. Status Solidi* 250 (6) (2013) 1128–1141.
- [39] J.D. Evans, L. Bocquet, F.-X. Coudert, Origins of negative gas adsorption, *Inside Chem.* 1 (6) (2016) 873–886.
- [40] J.D. Evans, J.P. Dürholt, S. Kaskel, R. Schmid, Assessing negative thermal expansion in mesoporous metal–organic frameworks by molecular simulation, *J. Mater. Chem. A* 7 (41) (2019) 24019–24026.
- [41] T.F. Willems, C.H. Rycroft, M. Kazi, J.C. Meza, M. Haranczyk, Algorithms and tools for high-throughput geometry-based analysis of crystalline porous materials, *Microporous Mesoporous Mater.* 149 (1) (2012) 134–141.
- [42] R.L. Martin, B. Smit, M. Haranczyk, Addressing challenges of identifying geometrically diverse sets of crystalline porous materials, *J. Chem. Inf. Model.* 52 (2) (2012) 308–318.
- [43] P.G. Boyd, S.M. Moosavi, M. Witman, B. Smit, Force-field prediction of materials properties in metal–organic frameworks, *J. Phys. Chem. Lett.* 8 (2) (2017) 357–363.
- [44] S. Plimpton, Fast parallel algorithms for short-range molecular dynamic, *J. Comput. Phys.* 117 (1) (1995) 1–19.
- [45] J.W. Morris, C.R. Krenn, The internal stability of an elastic solid, *Philos. Mag. A* 80 (12) (2000) 2827–2840.
- [46] S.J. Clark, M.D. Segall, C.J. Pickard, P.J. Hasnip, M.I.J. Probert, K. Refson, M. C. Payne, First principles methods using CASTEP, *Z. für Kristallogr. - Cryst. Mater.* 220 (5/6) (2005).
- [47] J.P. Perdew, K. Burke, M. Ernzerhof, Generalized gradient approximation made simple, *Phys. Rev. Lett.* 77 (18) (1996) 3865–3868.
- [48] M. Erkarta, M. Durandurdu, Pressure-induced amorphization of MOF-5: a first principles study, *ChemistrySelect* 3 (28) (2018) 8056–8063.
- [49] A.U. Ortiz, A. Boutin, A.H. Fuchs, F.-X. Coudert, Investigating the pressure-induced amorphization of zeolitic imidazolate framework ZIF-8: mechanical instability due to shear mode softening, *J. Phys. Chem. Lett.* 4 (11) (2013) 1861–1865.
- [50] D. Machon, F. Meersman, M.C. Wilding, M. Wilson, P.F. McMillan, Pressure-induced amorphization and polyamorphism: inorganic and biochemical systems, *Prog. Mater. Sci.* 61 (2014) 216–282.
- [51] M. Erkarta, M. Durandurdu, Pressure-induced amorphization, mechanical and electronic properties of zeolitic imidazolate framework (ZIF-8), *Mater. Chem. Phys.* (2020) 240.
- [52] M. Parrinello, A. Rahman, Strain fluctuations and elastic constants, *J. Chem. Phys.* 76 (5) (1982) 2662–2666.
- [53] J. Wieme, L. Vanduyfhuys, S.M.J. Rogge, M. Waroquier, V. Van Speybroeck, Exploring the flexibility of MIL-47(V)-Type materials using force field molecular dynamics simulations, *J. Phys. Chem. C* 120 (27) (2016) 14934–14947.
- [54] S.M. Rogge, J. Wieme, L. Vanduyfhuys, S. Vandenbrande, G. Maurin, T. Verstraelen, M. Waroquier, V. Van Speybroeck, Thermodynamic insight in the high-pressure behavior of UiO-66: effect of linker defects and linker expansion, *Chem. Mater.* 28 (16) (2016) 5721–5732.
- [55] J.C. Tan, B. Civalleri, C.C. Lin, L. Valenzano, R. Galvelis, P.F. Chen, T.D. Bennett, C. Mellot-Draznieks, C.M. Zicovich-Wilson, A.K. Cheetham, Exceptionally low shear modulus in a prototypical imidazole-based metal–organic framework, *Phys. Rev. Lett.* 108 (9) (2012), 095502.
- [56] J.M. Gere, S.P. Timoshenko, *Mechanics of Materials*, Nelson Thornes Ltd, 1991.
- [57] A.K.C.C.J. Rappé, K.S.U.F.F. Cowell, A full periodic table force field for molecular mechanics and molecular dynamics simulations, *J. Am. Chem. Soc.* 114 (25) (1992) 10024–10035.
- [58] S.M.J. Rogge, S. Caroës, R. Demuynck, M. Waroquier, V. Van Speybroeck, A. Ghysels, The importance of cell shape sampling to accurately predict flexibility in metal–organic frameworks, *J. Chem. Theor. Comput.* 14 (3) (2018) 1186–1197.
- [59] L.R. Redfern, L. Robison, M.C. Wasson, S. Goswami, J. Lyu, T. Islamoglu, K. W. Chapman, O.K. Farha, Porosity dependence of compression and lattice rigidity in metal–organic framework series, *J. Am. Chem. Soc.* 141 (10) (2019) 4365–4371.
- [60] J. Zhang, Phase transformation in two-dimensional covalent organic frameworks under compressive loading, *Phys. Chem. Chem. Phys.* 20 (46) (2018) 29462–29471.
- [61] S. Krause, J.D. Evans, V. Bon, I. Senkovska, S. Ehrling, U. Stoeck, P.G. Yot, P. Iacomi, P. Llewellyn, G. Maurin, F.-X. Coudert, S. Kaskel, Adsorption contraction mechanics: understanding breathing energetics in isoreticular metal–organic frameworks, *J. Phys. Chem. C* 122 (33) (2018) 19171–19179.
- [62] R. Louis, M.D. Redfern, Megan C. Wasson, Lee Robison, Florencia A. Son, François-Xavier Coudert, Omar K. Farha, Isolating the role of the node-linker bond in the compression of UiO-66 metal–organic frameworks, *Chem. Mater.* 32 (2020) 5864–5871.
- [63] S. Krause, J.D. Evans, V. Bon, I. Senkovska, S. Ehrling, P. Iacomic, D.M. Többens, P. L. Llewellyn, D. Wallacher, M.S. Weiss, B. Zheng, P.G. Yot, G. Maurin, F.-X. Coudert, S. Kaskel, Engineering micromechanics of soft porous crystals for negative gas adsorption, *Chem. Sci.* 11 (2020) 9468–9479.